Final Technical Report

USGS/NEHRP Award No: G09AP00132

Towards Real-Time Double-Difference Event Relocation at the NEIC

Principal Investigator: Felix Waldhauser
Co-PI: David Schaff

Lamont-Doherty Earth Observatory of Columbia University
Palisades, NY 10964
Tel: (845) 365 8538; Fax: (845) 365 8150
felixw@ldeo.columbia.edu

Project Period: 09/01/2009 – 08/31/2010 (NFE: -08/31/2011)

Research supported by the U.S. Geological Survey (USGS), Department of the Interior, under USGS award number 07HQGR0044. The views and conclusions contained in this document are those of the authors and should not be interpreted as necessarily representing the official policies, either expressed or implied, of the U.S. Government.

Final Technical Report

USGS/NEHRP Award No: G09AP00132

Towards Real-Time Double-Difference Event Relocation at the NEIC

Principal Investigator: Felix Waldhauser
Co-PI: David Schaff

Lamont-Doherty Earth Observatory of Columbia University
Palisades, NY 10964
Tel: (845) 365 8538; Fax: (845) 365 8150
felixw@ldeo.columbia.edu

SUMMARY

We performed research towards building real-time double-difference location capability at the NEIC for earthquakes recorded at global seismic networks. Specifically, we have developed new procedures to perform comprehensive global-scale relocation of seismicity reported in standard earthquake bulletins. A global double-difference base catalog, relative to which new events are located with the DD-RT (double-difference in real-time) software package, is the most crucial item still missing in the teleseismic DD-RT system. Under this grant we developed a multi-step, multi-phase double-difference procedure that can handle the large location errors, especially in depth, in standard earthquake catalogs such as those generated by the ISC and NEIC. We tested these new algorithms by applying them to the aftershocks of the 2010 M_w7.0 Haiti and the 2004 M_w9.2 Sumatra-Andaman earthquakes. In both cases we are able to resolve the active fault structures at the scale of a few km or better. In the case of Haiti we show that moment release shifted from dominantly sinistral in the main rupture along the Enriquillo-Plantain Garden (EPGF) transform fault, to thrusting on SSW-dipping faults flanking the EPGF during the aftershocks. The results suggest that this transition may be caused by restraining bends at the ends of the main rupture where EPGF slip would raise fault-normal compression, heal it, and activate neighboring thrust faults. Relocations of a dense cluster of aftershocks off-shore northern Sumatra resolve splay faults that may have been re-activated post-seismically by ascending fluids released from the subducting oceanic crust along inherited sea floor fabric. Both cases demonstrate the usefulness of having such high-precision earthquake locations computed in real-time, as they provide important information that may help assess and mitigate hazards after the occurrence of major earthquakes.

1. Overview of Investigations

This final report covers the activities performed between September 1, 2009 (start date of the project) and August 31, 2010 (NFE until August 31, 2011). The work described here is being undertaken by the principle investigator Felix Waldhauser and by co-PI David Schaff.

The proposal was to perform work towards near-real-time double-difference location capability for earthquakes recorded by global seismic stations at regional and teleseismic distances. We made significant progress towards this goal, in particular towards the development of a global base catalog, which is an integral and crucial part of the real-time double-difference platform DD-RT. The DD-RT system, which has been developed for locally recorded earthquakes and operates currently on earthquakes in northern California, relocates new events relative to a high-precision double-difference base catalog (Waldhauser and Schaff, 2008), using cross-correlation and picks to estimate delay-time between a new event and reference events in the base catalog, and a single-event double-difference algorithm (Waldhauser, 2009) to relocate a new event relative to its reference events. Within the scope of this project we have developed new procedures for comprehensive relocation of global seismicity, which we tested on recent, globally recorded aftershock sequences and which we are currently using for computation of a global DD base catalog. In the following we are describing the new procedures and show results from applying them to the recent great earthquakes, including the 2004 Sumatra-Andaman and the 2010 Haiti earthquakes. Since the DD-RT software has been developed as a scale-independent system, a global DD base catalog is the most important missing piece towards real-time global DD relocation.

2. Investigations undertaken

New procedures for developing a comprehensive global double-difference catalog

A major challenge in applying double-difference procedures to the entire ISC and EDR bulletin data are the often large location uncertainties, especially the large number of earthquakes for which depths are not resolved and set to default values. Events with large location uncertainties and/or default depths may lead to an incomplete network of delay time links because their distance from their true neighbors is far greater than the threshold used to set up reasonable sized networks. Furthermore, since the double-difference algorithm minimizes residuals in a least-squares sense, a large number of grossly mislocated initial locations jeopardize the robustness of the inversion process and may also affect the precision of well-constrained events.

To circumvent these issues we have developed a new, multi-step relocation procedure that improves the large location errors in global catalog locations prior to the simultaneous double-difference inversion (Waldhauser et al., 2012). In a first step a reference catalog of well-constrained earthquake locations is established by simultaneous (i.e., regular) double-difference relocation of events with depths constrained by depth-phases in the EHB catalog (Engdahl et al. 1998). The resulting DD-EHB catalog is subsequently used as a base catalog, relative to which each event in the combined ISC and EDR catalogs is relocated one at a time using a single-event double-difference relocation algorithm, *hypoDDse*. In this iterative procedure, which has been originally designed for real-time double-difference location (Waldhauser, 2009), delay times are formed between an ISC/EDR event and a set of reference events in the DD base catalog, and the data are inverted for the precise location of that event relative to its reference events. The

hypoDDse inversion, helped by teleseismically recorded mantle and core phases with steep take-off angles, relocates default depths relative to reference events with well-constrained absolute depths. The resulting DDse catalog is then relocated via simultaneous teleseismic double-difference inversion of the ISC/EDR bulletin picks and cross-correlation delay times (Waldhauser and Schaff, 2007).

The step-wise improvement of this procedure is demonstrated in Figure 1 and Table 1 for ~1000 events off-shore northern Sumatra. Location differences in residuals decrease with each relocation step. Final DD locations have average horizontal differences of 12 km with respect to the original ISC locations, and ~7 km with respect to the DDse solutions. Differences between the final DD locations and the 168 depth-phase constrained EHB locations (Engdahl et al., 2007) are less than 5 km.

Table 1 Step-wise relocation using ISC bulletin data. Means and standard deviations (in km) between final DD locations in a cluster of teleseismically recorded earthquakes in northern Sumatra and corresponding ISC locations, single-event double-difference locations (DDse), and depth-phase constrained EHB locations. Directions are east-west (DX), north-south (DY) and vertical (DZ). Values in parentheses are number of events used for the statistics. NM: Not meaningful because of ISC default depths.

	std(DX)	std(DY)	std(DZ)	mean(|DX|)	mean(|DY|)	mean(|DZ|)
DD-ISC (1191)	16.7	14.3	*NM*	12.2	12.2	*NM*
DD-DDse (1191)	12.9	10.5	8.5	8.0	6.9	6.2
DD-EHB (168)	7.3	6.4	4.8	5.3	5.0	3.7

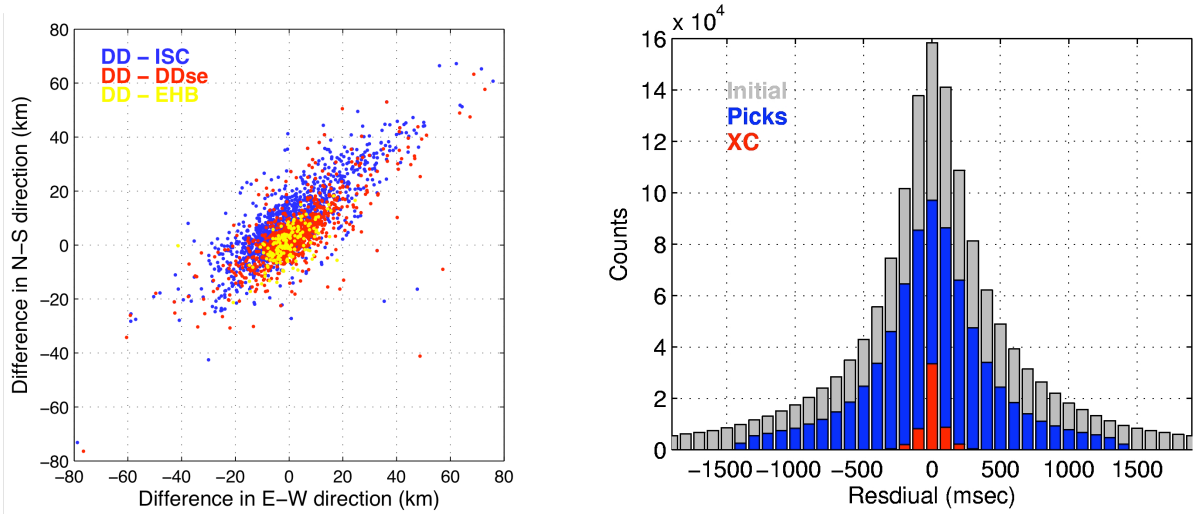

Figure 1 a) Differences in horizontal directions between final DD locations and ISC, DDse, and EHB locations for 1000 events in northern Sumatra recorded by regional and teleseismic stations. b) Residual distribution before and after relocation of the 1000 Sumatra events.

Application to the Sumatra-Andaman subduction zone

We have tested and applied the new step-wise, multi-phase cross-correlation based double-difference procedures in the Sumatra-Andaman region. While the development of the new procedures has been supported by this USGS grant, their application to the Sumatra-Andaman seismicity has been supported by an NSF grant. Nevertheless, we give here a brief summary of the findings as they highlight the performance of the new teleseismic double-difference procedures.

We relocated some 16,000 earthquakes out of close to 19'000 events in the combined ISC and EDR bulletins between 3°S - 17°N Latitude and 90°E - 102°E Longitude, covering the period from January 1964 to December 2008. An example set of pick and correlation data for ~1000 events off-shore northern Sumatra are shown in Figure 2, correlated seismograms generated by events in the same area in Figure 3d, and correlation results for the entire region are shown in Figure 3c (with colors indicating number of events with correlated seismograms). Figure 3c indicates that correlated events are located predominately along the plate interface and in regions of clustered seismicity (east of Nicobar Islands and in the Andaman back-arc). The Sumatra Fault System in northern Sumatra is characterized by the absence of correlated events.

The final DD locations for 16,000 events (Figure 3b) have rms residuals of 0.341 s (initial rms = 0.693 s) for the bulletin picks and 0.053 s for the cross-correlation data. Relative location uncertainties at the 95% confidence level derived from a bootstrap analysis have medians of a few kilometers both laterally and vertically. Formal least-squares for the best-constrained events (> 40 delay time links) in a dense cluster off-shore northern Sumatra are on average 1 km laterally and 1.5 km vertically. We used grid search methods together with a 3-D regional Vp model (Widiyantoro and Van der Hilst, 1996) to constrain and assess the accuracy of the absolute locations. We find that the bias caused by the regional 3D structure in the selected regions described below is typically less than a few km.

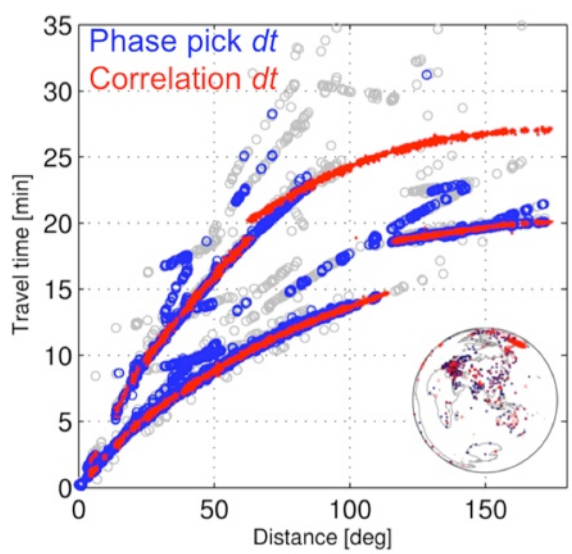

Figure 2 Example phase travel time curves showing all available phase arrival time picks in the ISC/EDR catalogs for aftershocks off-shore northern Sumatra (gray dots). Blue circles are phase arrival times observed pairwise at common stations and used to form pick delay times, and red dots are phases for which we measured correlation delay times. Inset: Distribution of stations used to relocate the events. Blue squares: station with pick delay times. Red squares: stations with correlation delay times.

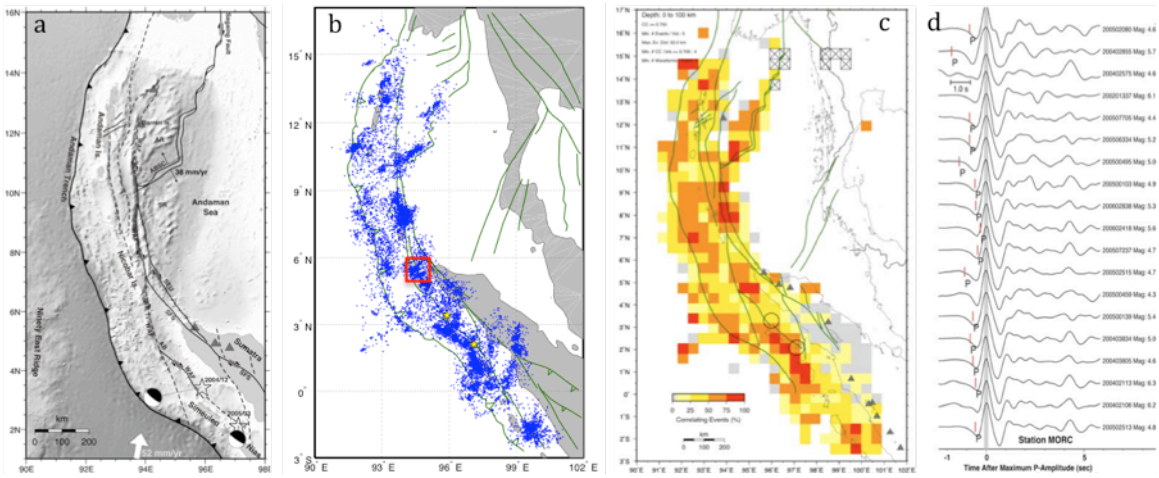

Figure 3 a) Simplified tectonic map of the Sumatra-Andaman region with active and inactive faults indicated by solid and dashed lines, respectively (after Curray, 2005). Convergence rate is from Sieh and Natawidjaja (2000). Stars denote NEIC epicenters of the December 2004 Sumatra-Andaman and March 2005 Nias event. CMT solutions plotted at centroid locations. Triangles denote volcanic arc. b) Double-difference locations of ~16'000 earthquakes. Red box denotes location of **Figure 4**a. c) Percentage of events with correlated seismograms within bins of 50 x 50 km. d) Example of correlated seismograms from aftershocks located off-shore northern Sumatra. (From Diehl et al., in prep.)

We summarize here the results from a detailed analysis of a subset of ~1000 earthquakes in a localized area off-shore northern Sumatra (Waldhauser et al., 2012) to demonstrate the level of location precision we achieve and the opportunity these new data present to gain insight into detailed earthquake and tectonic processes. The aftershocks locate ~200 km east of the Sunda Trench beneath the Aceh back arc basin, which is bounded on its western border by the NNW striking, right-lateral West Andaman fault (WAF) (see red box in Figure 3b). The general pattern of the aftershock distribution shows NE oriented lineations (or streaks), up to 80 km long and only a few km wide, separated by sparsely seismic zones (Figure 4a). The two most prominent streaks occur in the northern part of the study area. Some sections of the streaks are formed by short, NNE striking features, or sub-streaks.

A NE oriented cross-section along the two dominant streaks (2-2' in Figure 4a) indicate that the majority of hypocenters occur both on or near the plate interface and throughout the overriding Sunda plate (Figure 4b). The plate interface, as inferred from the relocated seismicity, steepens from 10° at the Sunda trench to ~30° beneath the eastern border of the Aceh basin, and is consistent with the plate geometry derived from a combined inversion of Wadati-Benioff earthquakes and local reflection profile data (Hayes and Wald, 2009). Between ~20 and 50 km depth they form steeply NE dipping structures that connect at their base with the plate interface (blue arrows in Figure 4b).

CMT solutions show predominately thrust motion on planes striking NW parallel to the trench and perpendicular to the orientation of the streaks (Figure 4b). Assuming the shallowly, NE dipping nodal plane is the active fault plane, fault dips for events along the plate interface continuously increase from ~15° on the trench side of the cross section to ~33° near the downdip

extent of the seismogenic mega-thrust, consistent with the deepening slab interface inferred from the relocated seismicity. Focal mechanisms for events above the plate interface also show NE dipping thrust mechanisms, suggesting that they represent slip on NW striking imbricate faults.

A spatio-temporal analysis of these aftershocks suggests that they are caused by fluids moving upwards along preexisting weak zones within the overriding plate. Figure 5a shows hypocenter depths plotted relative to the plate interface as a function of time (gray dots). The distribution is shown for three time intervals at increasingly compressed time scales. Mean depths (black dots) within bins of 2, 14, and 60 days of data indicate five periods with clear trends of ascending hypocenters. We estimate the rate of fluid flow, as expressed by the ascending earthquakes, by a least square fit of all data within each of the five periods (gray lines, Figure 5a), yielding correlation coefficients of ~0.3 at ~99% significance. Flow rates decrease exponentially from 569 m/day 12 days to 18 m/day 3 years after the mainshock (Figure 5b). We obtain similar rates with earthquakes along the two streaks only (dashed line in Figure 5b).

Permeabilities estimated from the fluid flow rates (Townend and Zoback, 2000) are in the range of 2.5×10^{-10} to 2.5×10^{-13} m^2. These are many orders of magnitudes larger than permeabilities for intraplate crust (Townend and Zoback, 2000) and accretionary wedges elsewhere in the world (Koerner et al., 2004). However, the existing network of imbricate faults and the generation of new fractures are likely to provide highly permeable pathways for fluids released from the subducting slab. Furthermore, as suggested by the exponential decay of fluid flow rate with time (Figure 5a), the extent and magnitude of shaking during the main shock may have temporarily increased permeability. The robustness of timing and rate of the fluid movement across the OBA area suggests that fluid release is controlled by some regionally acting process such as afterslip. About 30% additional (aseismic) fault slip occurred in the 1.5 months following the main rupture (Chlieh et al., 2007). Furthermore, the onset of the fluid flow event #2 (at 90 days) correlates with the occurrence of the Mw 8.6 Nias Island earthquake of 28 March 2005 (arrow in Figure 5a), suggesting that the release of fluids from the subducting plate may have been dynamically triggered.

These results lead us to the following conclusions, summarized here briefly and described in detail in Waldhauser et al. (2012): 1) The pattern of NE and NNE oriented streaks of epicenters (Figure 4a) may represent inherited sea floor fabric consistent with fracture zones of similar orientation that exist off-shore in the Wharton basin. 2) Fluids are expelled along these structures into the overriding crust, rise, and lower frictional strength along preexisting imbricate faults. 3) Location, correlation, and kinematic data of the largest events indicate that they occur on a splay fault that branches off the plate interface at about 55 km depth and surfaces at the western border of the forearc ridge where active thrust faults have been mapped after the 2004 mainshock (Lin et al., 2009; Sibuet et al., 2007; Figure 4b). 4) Significant slip during the mainshock may have occurred on the master-splay inferred from our aftershock analysis, contributing to the cataclysmic secondary near-field tsunami that was postulated to have originated near the forearc ridge based on early tsunami arrival times and high run-up heights (Plafker et al., 2006) and double-peaked lead waves recorded on the transects of Jason-1 satellite (Smith et al., 2005).

The correlation of the spatio-temporal distribution of the relocated aftershocks with independent geophysical and geological data and inferred processes confirm the high accuracy with which we are able to relocate earthquakes in global catalogs using our tools, and demonstrate the interesting features they are able resolve.

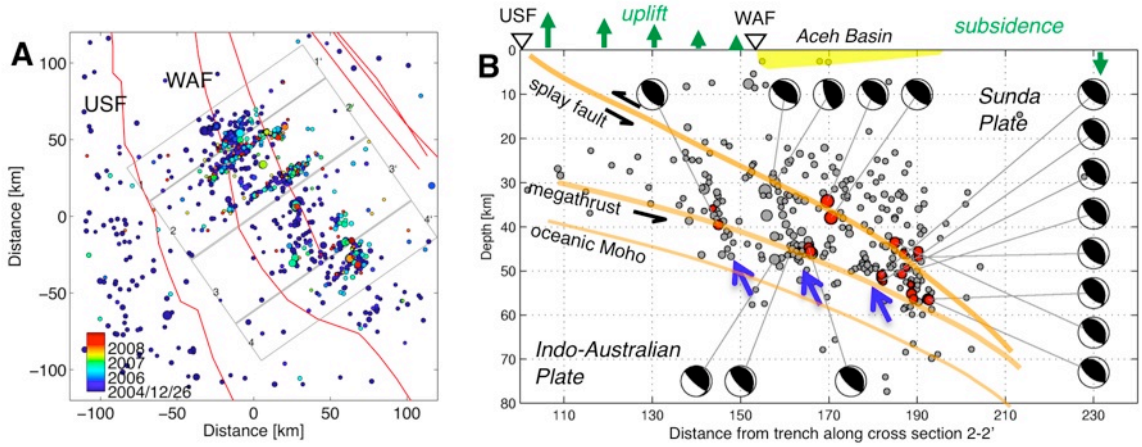

Figure 4 A: Map view of relocated aftershocks. Color scale indicates year of occurrence, circle size scales with magnitude. Rectangle 2-2' includes events shown in (B). Note NE and NNE orientations of aftershocks. B: Depth-distribution of hypocenters (dots) along 2-2'. No vertical exaggeration. Circle size scales with magnitude (range: Mw2.2-Mw6.2). CMT Focal mechanisms are lower hemisphere projections, red dots strongly correlated events, triangles locations of faults at surface, yellow area Aceh basin; orange lines inferred plate interface and master splay fault, green arrows geodetically observed uplift/subsidence (Chlieh et al., 2007), and blue arrows point to fluid paths. USF: Upper Splay Fault (Lin et al., 2009); WAF: West Andaman Fault.

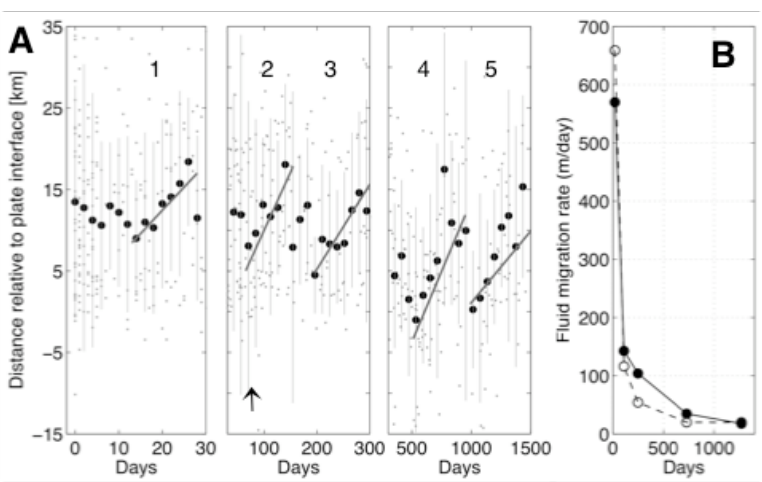

Figure 5 A: Time of aftershock occurrence (days) as a function of distance from the plate interface for 3 time intervals: days 0-30 after the mainshock (left), days 30-300 (center), and days 300-1500 (right). Black dots are mean depths within bins of 2 (left), 14 (center), and 60 days (right), thin gray lines associated standard deviations. Thick gray lines are least squares fit to all data (gray dots) within each of the five inferred fluid flow events (1-5) determined from the mean depth distribution (see text). Arrow denotes occurrence of the Mw 8.6 Nias Island earthquake. B: Fluid flow rates taken from the least squares fits in (A) plotted as a function of days (mean within period) after the mainshock. Solid line is for all events, dashed line for those within cross section 2-2' only.

Application to the 2010 Haiti earthquake

In response to the devastating 2010 M7.0 Haiti earthquake we have relocated, in near-real-time, its aftershock sequence as it progressed, and, together with Nano Seeber (LDEO), we have studied the aftershock distribution within a seismo-tectonic context. We have communicated our results and updates thereof to USGS and UN personnel in order to help assess the potential hazard associated with major aftershocks. A paper of this study is in review with Geology (Seeber et al., in prep), and what follows is a summary of the main findings.

The NEIC routine aftershock locations lack resolution much below the scale of the rupture, particularly in depth. We greatly improved hypocenter resolution for the mainshock and 75 aftershocks (Mw 4.2-5.9; Jan-Sep 2010) by applying the teleseismic double-difference algorithm of Waldhauser and Schaff (2007) to NEIC phase arrival times. In addition, we cross-correlated seismograms of all events in the sequence, but none correlated significantly, providing further evidence of a complex rupture. We decreased RMS residuals from 0.8 s before to 0.6 s after relocation, and obtained relative location uncertainties at the 90% confidence level are generally <2km laterally and vertically (Figure 6).

Relocated aftershocks are concentrated in two clusters centered near restraining bends 30 km apart along the EPGF (Figure 6), approximately the inferred main rupture length (Hayes et al., 2010). The western cluster and restraining bend are more prominent. Despite the wide spatial distribution, focal mechanisms for the aftershocks consistently show thrusting on WNW planes, in contrast with the WSW strike and large left component for the main rupture and EPGF. The mainshock epicentre is in the eastern cluster and near the only 3 aftershocks with similar mechanisms. The distribution of most hypocenters in this cluster is consistent with the steep north-dipping nodal plane of the mainshock, but the number is small and resolution poor.

In vertical sections normal to the strike of nodal planes (Figure 6b,c), the western cluster is resolvably broader than expected for a single fault and implies thrust faulting on either side of the EPGF. When hypocenters are tentatively grouped in Figure 6a, views along the slightly different average strikes of south-dipping nodal planes show multiple bands of hypocenters matching SSW-dipping thrust faults. North of the EPGF, the Trois Baies fault system was mapped offshore from reflection profiles (Momplaisir, 1986). It is a NNE-verging imbricate fault system that probably controls the steep southern flank of the Canal du Sud where water depth reaches 1700m. Folding of shallow turbidites at the base of this slope implies Holocene activity on this fault system. The Trois Baies fault is thus well positioned to account for the aftershocks in the western cluster north of the EPGF (green and dark blue in Figure 6).

South of the EPGF, several lines of evidence suggest a regional fault, SW-dipping and mostly blind, that we provisionally name the Jacmel thrust-fold. This fault has been mapped in segments across the southern peninsula from the Tapion Ridge on the northern coast to Jacmel Bay on the southern coast (Figure 6a) and interpreted as a single fault by Frydecki et al. (1989). It follows the Jacmel depression, which was a seaway as late as the Pliocene (Maurasse, 1982) and is probably an older structure reactivated in the Plio-Quaternary (Momplaisir, 1986). The Jacmel fault thrusts the Massif Hotte eastward onto the Massif Selle, two distinct regional morphotectonic units. The implied NE vergence and SW dip of the fault are consistent with the regional fabric south of the EPGF (e.g., Pubellier et al., 2000) and with the prominent bathymetric feature that marks the SE extension of the structure offshore. Mann et al. (1995) identify the Jacmel depression and the topographic and structural high Massif Hotte as a syncline-anticline pair. A similar pair 130 km west of the Jacmel structure (west of Figure 6) intersects the EPGF and is also associated with a restraining bend and push-up. A WNW-striking

fault mapped between the Tapion push-up and the Massif Hotte is probably an imbricate of the Jacmel fault (Figure 6a), while the most active basal structure responsible for the push-up is inferred to merge with the EPGF offshore, north of the push-up. The Jacmel fault is tentatively correlated with the light blue hypocenters in Figure 6c.

Our interpretation of SSW-dipping thrust faults on both sides of the EPGF associated with the western aftershock cluster in the 2010 sequence implies west-plunging intersections between these faults and the EPGF. A vertical EPGF would intersect a 50°-dipping Jacmel fault along a 45° west plunge (Figure 7A,B). Geometric asperities on transcurrent faults, such as bends, tend to evolve asymmetrically moving with the footwall side of these faults (Choi et al., 2011), which would be the south side of the EPGF according to the moment-tensor solution (Figure 6A). In this case, the bend on the EPGF is fixed at the intersection with the Jacmel fault. Even a slow rate on this fault can develop and maintain the bend. In contrast, the Trois Bais fault north of the EPGF moves past the bend and accommodates the bend rather than changing the shape of the EPGF.

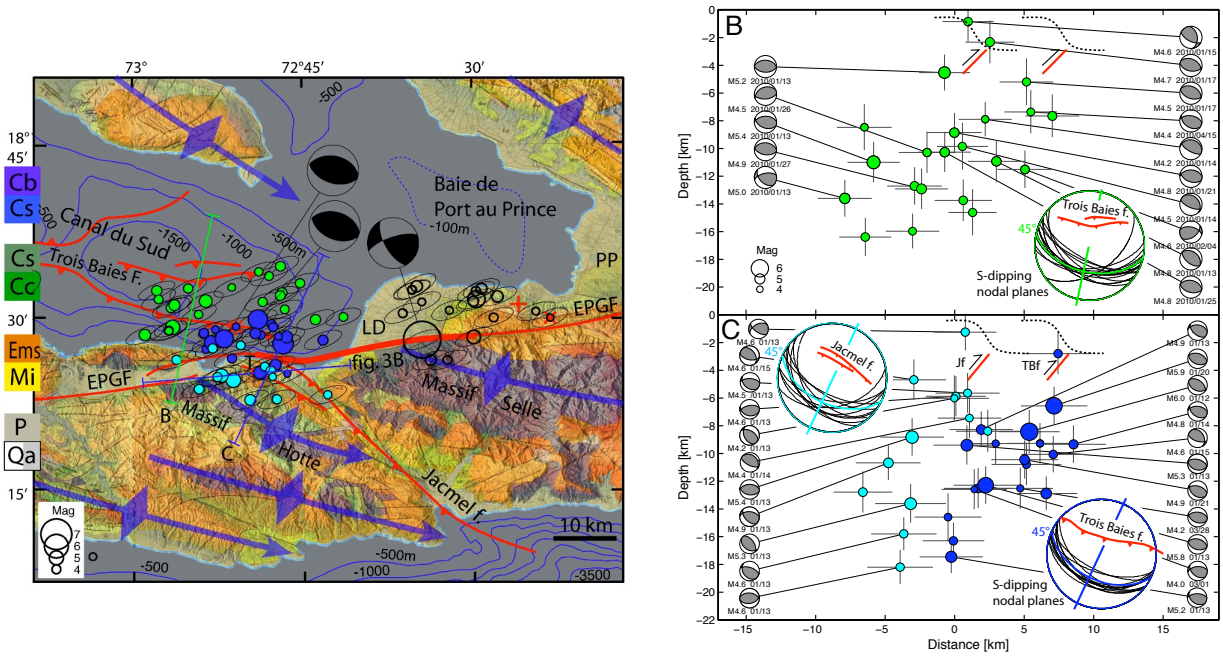

Figure 6 A: Portion of the southern peninsula of Haiti centered on the 2010 M7 earthquake sequence. 75 relocated epicenters (1-9/2010; ellipses are 90% relative uncertainties) are clustered near the Enriquillo-Plaintain Garden fault (EPGF), marking the ends of the main rupture. In the western cluster they are color coded according to interpreted fault sources (see text). The red x and + identify epicenters from teleseismic DD and local stations, respectively, for two shared events. Only the one in the western cluster has a reliable local epicenter, which is used to place the DD epicenters. Geology from the Bureau of Mines and Energy of Haiti is draped on a Google Earth image. PP = Port au Prince; LD = Leogane Delta; Cb: Cretaceous oceanic igneous basement; Cs, Cc, EP, Ems, O: Cretaeous, Paleocene, Eocene, Oligocene carbonates; Mi: Miocene Flysh; P: Pliocene shallow marine sands; Qa: Quaternary alluvium and marine terraces. B and C are vertical sections of green and blue hypocenters, respectively (located in A). Sections are normal to average strike of south-dipping nodal planes in each group (insets). Moment-tensor solutions are in lower hemisphere map view.

Generally, both normal and thrust faults may interact with transcurrent faults along transtensive and transpressive boundaries. In both cases, however, their warping of the strike-slip fault is likely be restraining (Figure 7C). The feedback, therefore is positive in transpression, but negative in transtension. This fundamental asymmetry is likely to favor partitioning in transpression but to discourage it in transtension. The positive feedback between strike slip and thrusting along partitioned transpressive boundaries is expected to concentrate shortening close to the transform and to restraining bends at fault intersections. As the bends move at transform speed, the cumulative effect may account for the ridges that often characterize these boundaries. For example, the northern and southern transforms in western Hispaniola are associated with 5+ km high ridges, including the submarine part.

In summary, our fault intersection and feedback model of the 2010 sequence invokes seismogenesis only on well developed known faults and accounts for several key features, including: 1) self-silencing of the mainshock source and the shift to thrusting during the early aftershocks; 2) their clustering near the western end of the rupture and a restraining bend on the EPGF; 3) the west-dipping pattern of the western aftershocks co-located with the EPGF. This model may be applicable to other transpressive boundaries.

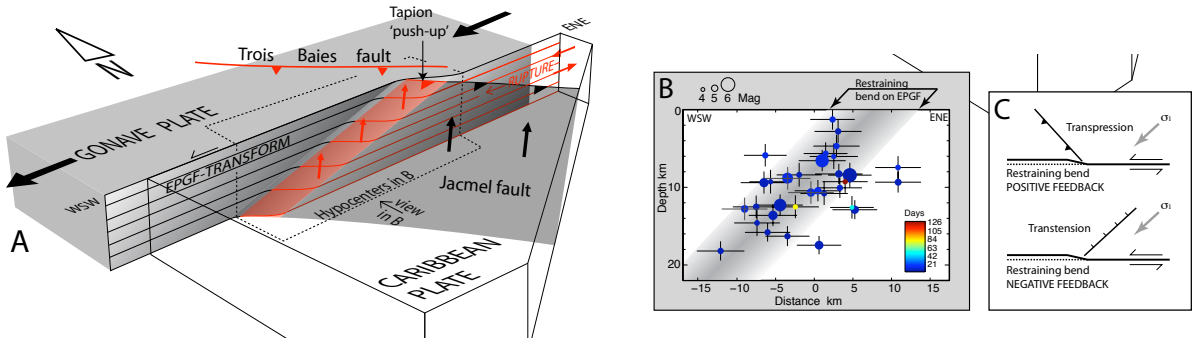

Figure 7 A: West-dipping restraining bend at the intersection between the EPGF and the Jacmel thrust fault. The January 12 rupture propagated westward on the EPGF to the bend where the constriction increased fault-normal stress, stopping the rupture and triggering thrust aftershocks on both sides of the EPGF. B: Hypocenters near the EPGF projected on an EPGF-parallel section,dark blue on Trois Baies fault and light blue on Jacmel fault(see **Figure 6**A,B). The latter forms a band dipping to the west, which is interpreted to mark the restraining bend. C: Generalized geometry and feedback at fault intersections in slip-partitioned transpressive and transtensive boundaries. Given the likely relative orientations of faults sharing the same stress field, a transcurrent master fault warps into a restraining bend at an intersection with any dip-slip fault. Strike slip through the bend will encourage further slip on the thrust fault, but discourage it on the normal fault.

3. References

Chlieh, M., J.-P. Avouac, V. Hjorleifsdottir, T.-R. A. Song, C. Ji, K. Sieh, A. Sladen, H. Hebert, L. Prawirodirdjo, Y. Bock, J. Galetzka, 2007, Coseismic Slip and Afterslip of the Great *M*w 9.15 Sumatra–Andaman Earthquake of 2004, *Bulletin of the Seismological Society of America* 97, 152–S173, doi: 10.1785/0120050631.

Choi, E. L. Seeber, M. Steckler, R. Buck, One-sided transform basins and "inverted curtains": Implications for releasing bends along strike-slip faults, Tectonics, in press.

Engdahl, E.R., R. van der Hilst, & R. Buland, Global teleseismic earthquake relocation with improved travel times and procedures for depth determination, *Bull. Seism. Soc. Am*., 22, 2317-2320, 1998.

Engdahl, E.R., A. Villasenor, H.R. DeShon, C.H. Thurber, 2007, Teleseismic Relocation and Assessment of Seismicity (1918–2005) in the Region of the 2004 *M*w 9.0 Sumatra–Andaman and 2005 *M*w 8.6 Nias Island Great Earthquakes, *Bulletin of the Seismological Society of America* 97, S43–S61, doi: 10.1785/0120050614.

Frydecki, J., M.L. Joseph, C.Jean-Poix, J.Krason, and M. Dominique Nuvel Apercu d'Exploration Petroliere en Haiti, Bureau des Mines et de L'energie, Haiti, Sus Programme II, Report by Geoesplorers International Inc. 38 pages, 1989.

Hayes, G.P. and D.J. Wald, 2009, Developing a framework to constrain the geometry of the seismic rupture plane on subduction interfaces *a priori* – a probabilistic approach, *Geophysical Journal International* 176, 951-964.

Koerner, A., E. Kissling, S.A. Miller, 2004, A model of deep crustal fluid flow following the Mw=8.0 Antofagasta, Chile, earthquake, *Journal of Geophysical Research* 109, B06307. doi:10.1029/2003JB002816.

Lin J.-Y., X. Le Pichon, C. Rangin, J.-C. Sibuet, T. Maury, 2009, Spatial aftershock distribution of the 26 December 2004 great Sumatra-Andaman earthquake in the northern Sumatra area, *Geochemistry Geophysics Geosystems* 10, doi:10.1029/2009GC002454.

Mann, P., F.W.Taylor, R. Lawlence-Edwards, The-Lung Ku. Actively evolving microplate formation by oblique collision and sideways motion along strike-slip faults: an example from the northwestern Caribbean plate margin, Tectonophysics 246, pp 1-69, 1995.

Maurrasse, F. Suvey of the geology of Haiti, Guide to field excursion 3-8 March 1982 sofia.usgs.gov/publications/reports/...maurrasse1982/pdf_index.html

Momplaisir, B.-A. R. Contribution a l'etude geologique de la partie orientale du massif de la Hotte, doctorate thesis of the University of Paris 6, 200pp, 1986.

Plafker, G., S. Nishenko, L. Cluff, M. Syahrial, 2006, The cataclysmic 2004 tsunami on NW Sumatra – preliminary evidence for a near-field secondary source along the western Aceh Basin, *Seismological Research Letters* 77, 231.

Pubellier, M., A. Mauffret, S.Leroy, J.-M. Vila, and H. Amilcar, Plate boundary readjustment in oblique convergence – Example of the Neogene of Hispaniola, Greater Antilles, Tectonics 19, 630-648, 2000.

Seeber, L., F. Waldhauser, T. Diehl, V. Hjorleifdottir, M. Nettles, The January 2010 Haiti mainshock-aftershock sequence: Positive feedback between faults in slip-partitioned transpression, *Geology*, 2012, in review.

Sibuet, J.-C., C. Rangin, X. Le Pichon, S. Singh, A. Cattaneo, D. Graindorge, F. Klingelhoefer, J.-Y. Lin, J.-A. Malod, T. Maury, J. Schneider, N. Sultan, M. Umber, H. Yamaguchi, 2007, 26th December 2004 great Sumatra-Andaman earthquake: Co-seismic and post-seismic

motions in northern Sumatra, *Earth and Planetary Science Letters* 263, 88-103. doi: 10.1016/j.epsl.2007.09.005
Smith, W.H.F., R. Scharroo, V.V. Titov, D. Arcas, B.K. Arbic, 2005, Satellite altimeters measure tsunami – early model estimates confirmed, *Oceanography* 18(2), 10-12.
Townend, J., M.D. Zoback, 2000, How faulting keeps the crust strong. *Geology* 28, 399–402.
Waldhauser, F. and D.P. Schaff, Regional and teleseismic double-difference earthquake relocation using waveform cross correlation and global bulletin data, *J. Geophys. Res.*, 112, B12301, doi:10.1029/2007JB004938, 2007.
Waldhauser, F. and D.P. Schaff, Large-scale relocation of two decades of Northern California seismicity using cross-correlation and double-difference methods, J. Geophys. Res., 113, B08311, doi:10.1029/2007JB005479, 2008.
Waldhauser, F., Near-real-time double-difference event relocation using long-term seismic archives, with application to Northern California, *Bull. Seism. Soc. Am.*, 2009, in review.
Waldhauser, F., D.P. Schaff, T. Diehl, and E.R. Engdahl, Splay faults imaged by fluid-driven aftershocks of the 2004 Mw 9.2 Sumatra-Andaman earthquake, *Geology*, 2012, in press.
Widiyantoro, S. and R.D. Van der Hilst, 1996, Structure and evolution of the subducted lithosphere beneath the Sunda arc, Indonesia, *Science,* 271, 1566-1570, doi:10.1126/science.271.5255.1566.

4. Papers/abstracts published related to this project

Papers:

Waldhauser, F., D.P. Schaff, T. Diehl, and E.R. Engdahl, Splay faults imaged by fluid-driven aftershocks of the 2004 Mw 9.2 Sumatra-Andaman earthquake, *Geology*, 2012, in press.
Seeber, L., F. Waldhauser, T. Diehl, V. Hjorleifdottir, M. Nettles, The January 2010 Haiti mainshock-aftershock sequence: Positive feedback between faults in slip-partitioned transpression, *Geology*, 2012, in review.

Abstracts:

McHugh, C.M., L. Seeber, M.-H. Cormier, M. Hornbach, R. Momplaisir, F. Waldhauser, C.C. Sorlien, M.S. Steckler, S. Gulick, A Seismo-Tectonic Signal From Offshore Sedimentation: The 2010 Haiti Earthquake and Prior Events, Abstract T33G-2492, Fall Meeting, AGU, San Francisco, Calif., 5-9 Dec, 2011.
Waldhauser, F., and D. Schaff, Real-time double-difference location and monitoring of fine-scale seismic properties, SSA Annual Meeting, *Seism. Res. Lett.* 81, 2, p.377, 2010.
Waldhauser, F., T. Diehl, N. Seeber, V. Hjorleifsdottir, and M. Nettles, High-resolution aftershock relocations and focal mechanisms of the 2010 Mw7.0 Haiti and Mw8.8 Chile earthquakes, SSA Annual Meeting, *Seism. Res. Lett.* 81, 3, 2010.
Seeber, L., F. Waldhauser, T. Diehl, V. Hjorleifsdottir, M. Nettles, The January 2010 Haiti mainshock-aftershock sequence: Positive feedback between faults in strain-partitioned transpression, Abstract U13A-0007, Fall Meeting, AGU, San Francisco, Calif., 13-17 Dec, 2010.
Seeber, N., and F. Waldhauser, The January 2010 Haiti mainshock-aftershock discrepancy: structural and stress interactions between faults in strain partitioned transpression, SSA Annual Meeting, *Seism. Res. Lett.* 81, 3, 2010.

Waldhauser, F., D. Schaff, E.R. Engdahl, and T. Diehl, Streaks of Aftershocks Following the 2004 Sumatra-Andaman Earthquake, *Eos Trans. AGU, 90*(52), AGU Fall Meet. Suppl., Abstract T24B-04, 2009.

Waldhauser, F., Real-Time Double-Difference Seismic Monitoring, *ES-SSA Annual Meeting,* October 5-6, Palisades, NY, 2009.